# Machine Learning-Assisted Bayesian Optimization for Discovery of Effective Additives for Dendrite Suppression in Lithium Metal Batteries

*Damien K. J. Lee[1], Teck Leong Tan[2] and Man-Fai Ng[2,*]*

[1]Department of Materials Science and Engineering, National University of Singapore, 9 Engineering Drive 1, 117575, Singapore

[2]Institute of High Performance Computing (IHPC), Agency for Science, Technology and Research (A*STAR), 1 Fusionopolis Way, #16-16 Connexis, Singapore 138632, Republic of Singapore

## ABSTRACT

In the pursuit of enhancing the performance and safety of Lithium (Li)-metal batteries, the discovery of effective electrolyte additives to suppress Li dendrites has emerged as a paramount objective. In this study, we employ an inverse design strategy to identify potential additives for dendrite mitigation. Two key mechanisms, namely the formation of robust solid electrolyte interphase (SEI) layers and the levelling mechanism, serve as the foundation for our investigation. Our inverse design strategy is guided by molecular properties such as the LUMO energy and interaction energy upon Li surface adsorption. An active learning process utilizing Bayesian Optimization (BO) was utilized to identify potential molecules with the ideal properties. Through this screening process, we uncover a collection of 146 molecules with the potential to act as SEI-forming additives, along with 13 molecules for levelling additives – both surpassing the performance of established additives reported in literature. This work highlights the potential of Bayesian Optimization methods in computational-based inverse design of materials for many applications, and the discovered additives could potentially boost the commercialization of Li-metal batteries.

## Introduction

Lithium (Li)-metal batteries (LMBs) have long been regarded as a highly promising battery technology, often considered to be the "holy grail" of Li battery technologies. When Li metal is used as the anode, it has an extremely high theoretical capacity (3860 mAh/g) and the lowest negative electrochemical potential (−3.040 V vs. Standard Hydrogen Electrode),[1–3] achieving the maximum possible energy density for the anode. However, LMBs remain largely infeasible due to safety issues arising primarily from the growth of Li dendrites during the electrodeposition of Li ions onto the metal surface.[4–6] These dendrites increase the risk of short-circuit, leading to thermal runway and risk of explosions. The graphite anode was ultimately commercialized in 1991 by Sony Corporation, sacrificing the theoretical capacity from 3860 mAh/g to 372 mAh/g,[7] but guaranteed dendrite-free operation and demonstrated remarkable success for over three decades.[8]

There remains an urgent need to increase the energy density of energy storage materials to enable widespread adoption of renewable energy sources and accelerate the transition towards a low-carbon economy, prompting a growing focus on research into making LMBs commercially feasible. Several strategies have been proposed to suppress dendrite growth,[9] such as solid-state electrolytes,[10–12] structured anode design,[13–15] electrolyte additives,[16–18] and artificial solid electrolyte interphase (SEI) design.[19,20]

Among these strategies, electrolyte additives are a cost-effective approach for mitigating the growth of Li dendrites during charge-discharge cycling of the battery. There have been various successes in previous studies in employing organic and inorganic molecules[21–26] and ionic salts[27–29] to achieve high Coulombic Efficiency (CE) and dendrite-free LMBs.[9] However, the characteristics of these additives and their dendrite-suppressing mechanisms vary greatly from one another. There is little insight on how to guide chemical design of novel additives. Experimental

synthesis and characterization are often time-consuming and yield varying degrees of success. High-throughput (HT) virtual screening, employing high-fidelity computations, has the potential to expedite the discovery of desired materials. To enable HT computational screening for promising electrolyte additives, a comprehensive understanding of the dendrite-suppression mechanism of such additives is first required, such that appropriate (chemical) descriptors can be identified.

Several mechanisms have been proposed to explain how additives suppress dendrite formation. The predominant mechanism exploited by most studies of electrolyte additives is to manipulate the solid electrolyte interphase (SEI) layer, which develops during the cycling stages of the battery. The characteristics of the SEI layer are instrumental to the morphological evolution of the Li anode during cell operation, whereby a stable and robust SEI layer is required to ensure the longevity of the Li anode. A dense high-modulus SEI layer acts effectively as a mechanical barrier to suppress Li dendrite formation.[30] Electrolyte additives modify the composition and properties of the SEI layer. Acting as sacrificial components, these additives are reduced on the Li anode surface, thereby preventing further reaction between the electrolyte with Li. The SEI film could consist of many chemical species, such as $Li_2CO_3$, LiF, $Li_2O$, $Li_3N$, $Li_2S$, $Li_3PO_4$, and Li alkylcarbonate,[9,31,32] depending on the composition of the electrolyte and additives. Several studies have provided evidence of certain additives, through their reductive decomposition, facilitating the formation of stable and dense SEI layers.[23,24,33,34] Recently, Yang et al. demonstrated 2,2,2-Trifluoroethyl trifluoroacetate (2,2,2-TFTF) to be effective in forming a robust SEI layer with 99.7% CE and Li dendrite suppression.[35] Using Density Functional Theory (DFT) calculations, they reported a lowest unoccupied molecular orbital (LUMO) energy level that is lower than common electrolytes and a high adsorption energy on Li surface, suggesting that 2,2,2-TFTF

tailors the SEI from dissociative adsorption. The low LUMO level and high adsorption energy facilitates the reduction of the additive on the Li anode surface, forming a dense SEI layer that suppresses dendrite growth.

Another mechanism for dendrite suppression is through the levelling effect of additives, which finds widespread use in the electroplating industry.[36,37] This effect involves the preferential deposition of metal ions on high-energy regions of the electrode surface, which helps to even out surface irregularities thereby promoting uniform metal ion deposition. A well-known example involves the incorporation of additives to ensure even deposition within high aspect ratio vias during copper electroplating in the microelectronics industry.[38,39] This class of additives show promise in reducing the likelihood of dendrite formation during the charging process of the battery. Wang et al. reported thiourea (THU) to be an effective leveller for the Li-metal anode, achieving stable cycling at a high current density for over 1000 cycles. They attributed this levelling effect to the reduced deposition energy for Li nucleation arising from THU adsorption. Through DFT calculations, they show that THU has a higher adsorption energy compared to electrolyte molecules, facilitating a more favorable surface for Li deposition.[40] Likewise, Lee et al. investigated the effectiveness of vinylpyrrolidone (VP) as a leveller where DFT calculations demonstrated that the VP additive preferentially adsorbs on high-energy sites, promoting surface reconstruction and facilitating flat plating during Li deposition.[41]

For the computational design of novel additives, we focus on the above two mechanisms – (i) the SEI formation via reductive decomposition and (ii) the levelling effect. These additives will be referred to as SEI additives and LL (leveller) additives respectively in this work.

From the above literature review, we identify the following desirable properties that promising additives should possess:

1. For the formation of the SEI layer (SEI additives), the additive should have a lower LUMO energy level than that of the electrolyte molecules, for preferential reduction on the Li metal surface.

2. For the additive to act as a leveller (LL additives), the LUMO energy level should be higher than that of the electrolyte molecules, which also improves anodic stability towards decomposition.[42] This prevents the reaction of the additive with the metallic Li surface to facilitate the levelling effect.

3. In both mechanisms, the additive should exhibit a larger (more negative) adsorption energy relative to electrolyte molecules. For SEI additives, the additive may undergo dissociative adsorption (chemisorption), whereas for LL additives, it is preferred that the additive remains intact during adsorption such that it can reversibly desorb from the Li surface. For the remainder of this manuscript, we refer to the adsorption energy as the *interaction energy* to encompass both cases of adsorption and dissociative adsorption.

The LUMO energies and interaction energies, calculable from DFT, serve as descriptors for high-throughput screening of additives from existing databases, from which we could develop inverse design strategies to identify promising electrolyte additives for further evaluation. Recent advancements in Machine Learning (ML) techniques have expedited the growth of data-driven materials design.[43–47] Bayesian Optimization (BO) is one type of active learning strategy and is an effective global optimization tool for black-box functions.[48] The method constructs a probabilistic ML surrogate model to represent the unknown objective function. By iteratively selecting the next point to evaluate based on an acquisition function that balances exploration and exploitation, BO intelligently explores the search space and narrows down the search region for the global optimum. At each iteration, the surrogate model is updated with new data, improving its accuracy; the

improved model is then used to suggest new evaluation points for subsequent iterations. BO techniques have been widely applied for the inverse design of molecules and materials, such as electrocatalysts,[49] photosensitizers,[50] redox flow batteries,[51] polymers,[52] to name a few examples.

In this study, we implement a BO process to screen for additives that inhibit the growth of Li dendrites (Figure 1) in Li-metal batteries. By leveraging on the largest open-source molecular database available,[53] we survey a search space of over 2.6 million molecules. Firstly, a randomly selected subset of molecules was labelled their respective LUMO energies, along with their calculated interaction energies on the (100), (110) and (111) surfaces of Li metal. This subset forms the initial training database for the surrogate model. Subsequently, we implemented a BO process that recommends molecules for further evaluation at each iteration to reduce the model's uncertainty or validate promising molecules with the desirable descriptors. These recommended molecules were then labelled with calculated properties and added to the training set. An active learning loop is formed in which the surrogate model iteratively improves while the algorithm converges towards the global optimum of the search space. We implement 2 independent BO processes, one each for the SEI additives and the LL additives. Our findings revealed 146 SEI additives and 13 LL additives as promising candidates that could outperform previously reported additives in the literature.

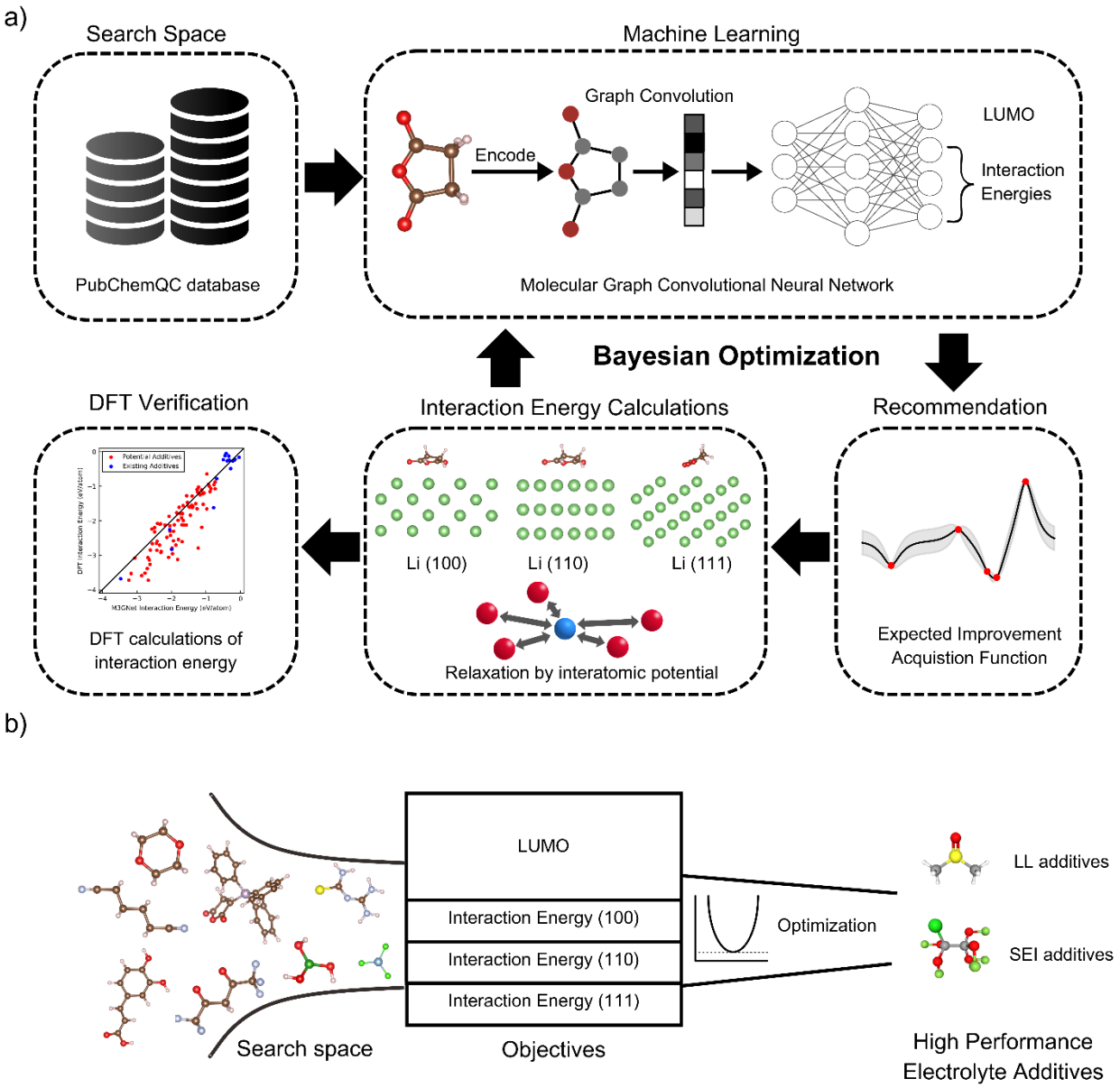


**Figure 1.** a) Workflow of the Bayesian Optimization (BO) process for discovery of high-performance electrolyte additives. b) Optimization scheme for inverse design of molecules. The relative heights of the respective objectives in the middle box are indicative of the weight given to the objective. The respective weights are found in Section S4 of the Supporting Information.

## Results

### Search space and labelling of molecules

Since there is no design rules to filter promising additive molecules based on structural features/descriptors, the search space for electrolyte additives potentially encompasses all ~$10^{60}$ molecules that are currently known.[54] The vast number of molecules renders a systematic computational screening infeasible. Therefore, we sought the largest general open-access database of molecules with calculated properties to provide a thorough screening of molecules without any structural bias. The PubChemQC database is currently the largest molecular database for this purpose, containing over 2.6 million molecules with optimized geometry and electronic properties computed at the B3LYP/6-31G* level.[53,55] The molecules are identified by their PubChem Compound Identification (CID) and their Simplified Molecular Input Line Entry System (SMILES) string. The CID is a unique identifier assigned to each compound in the PubChem database, while the SMILES string is a textual representation of the molecular structure. We performed a split of the database by their LUMO energy, where molecules with a LUMO less than 0 eV (i.e., to target the relatively more easily reduced molecules), form the search space for SEI additives. This subset consists of 1.8 million molecules. The remaining 0.8 million molecules form the search space for LL additives. The entire database consists of molecules containing 31 unique elements, ranging from a minimum of 1 atom to a maximum of 51 atoms for each molecule.

Obtaining accurate interaction energies of a large number of complex molecules on the surface of metallic Li from expensive DFT calculations poses a significant computational challenge. Here, we utilized a graph-based "universal" interatomic potential (M3GNet) recently developed by Chen and Ong[56] to perform interaction energy calculations. The M3GNet interatomic potential is trained from 89 elements in the periodic table and has been applied successfully in

molecular dynamics studies.[56] It offers a computationally cheaper way than quantum mechanical methods to obtain the energy of any relaxed structure (see Section 1 of Supporting Information), while retaining the accuracy of first-principles calculations. While numerous interatomic potentials have been extensively used in literature, these interatomic potentials require extensive training and are limited to specific chemistries for different applications. The M3GNet model provides a pretrained universal interatomic potential (zero-shot learning), which can be used for initial screening purposes with reasonable accuracy, and is more suited for our dataset where the molecules consist of diverse elements in the periodic table. We have also validated M3GNet-calculated interaction energies against the DFT-calculated ones (see Discussion section).

Over 500 configurations of molecule-adsorbed-surfaces were enumerated to identify those with strong interactions with the Li surfaces, taking into account the initial molecule orientations and different adsorption sites on the metal surface. Detailed information of our configuration generation algorithm is found in the Computational Methods section. The molecules were then labelled with the strongest interaction energy (i.e., the interaction energy produced from the most thermodynamically stable configuration, the state the molecule is most likely to be in) for the various surfaces.

**Machine Learning and Bayesian Optimization**

Two distinct surrogate models were trained for SEI additives and LL additives (SEI-model and LL-model, respectively). The initial labelled dataset used for the training and evaluation of the surrogates consists of 3043 and 1417 molecules, randomly selected from the PubChemQC database, for the SEI-model and LL-model respectively. These molecules were labelled with their LUMO energy and interaction energies on the Li surfaces. Each initial dataset is then split into training, validation, and test sets in the ratio of 80%, 10% and 10% respectively. Since graphs are

a natural representation of molecules, we considered graph-based deep learning model architectures[57,58] and evaluated them on the unbiased test set. The Molecular Graph Convolutional Neural Network[59] was chosen as the surrogate model as it achieves the lowest mean absolute error (MAE) on the test set for both the SEI-model and the LL-model (see Figure S1 in Supporting Information). Under this representation, atomic features such as atomic number, hybridization, etc. are encoded in each node. The graph convolution layers combine the feature vectors with neighboring nodes using several convolution operations, resulting in a molecular fingerprint. The molecular fingerprint was then passed to several fully connected layers to obtain the final predictions. The hyperparameters of both models were optimized using a Gaussian Process (see Table S1 in Supporting Information). Figures 2 and 3 show the performance of the model on the train, validation, and test sets of the optimized SEI-model and LL-model. The average MAE of the test set was 0.531 eV and 0.438 eV for the SEI-model and LL-model, respectively. The weighted average MAE (according to the weights defined in the next section, see below) of the test set is 0.442 eV and 0.362 eV for the SEI-model and LL-model.

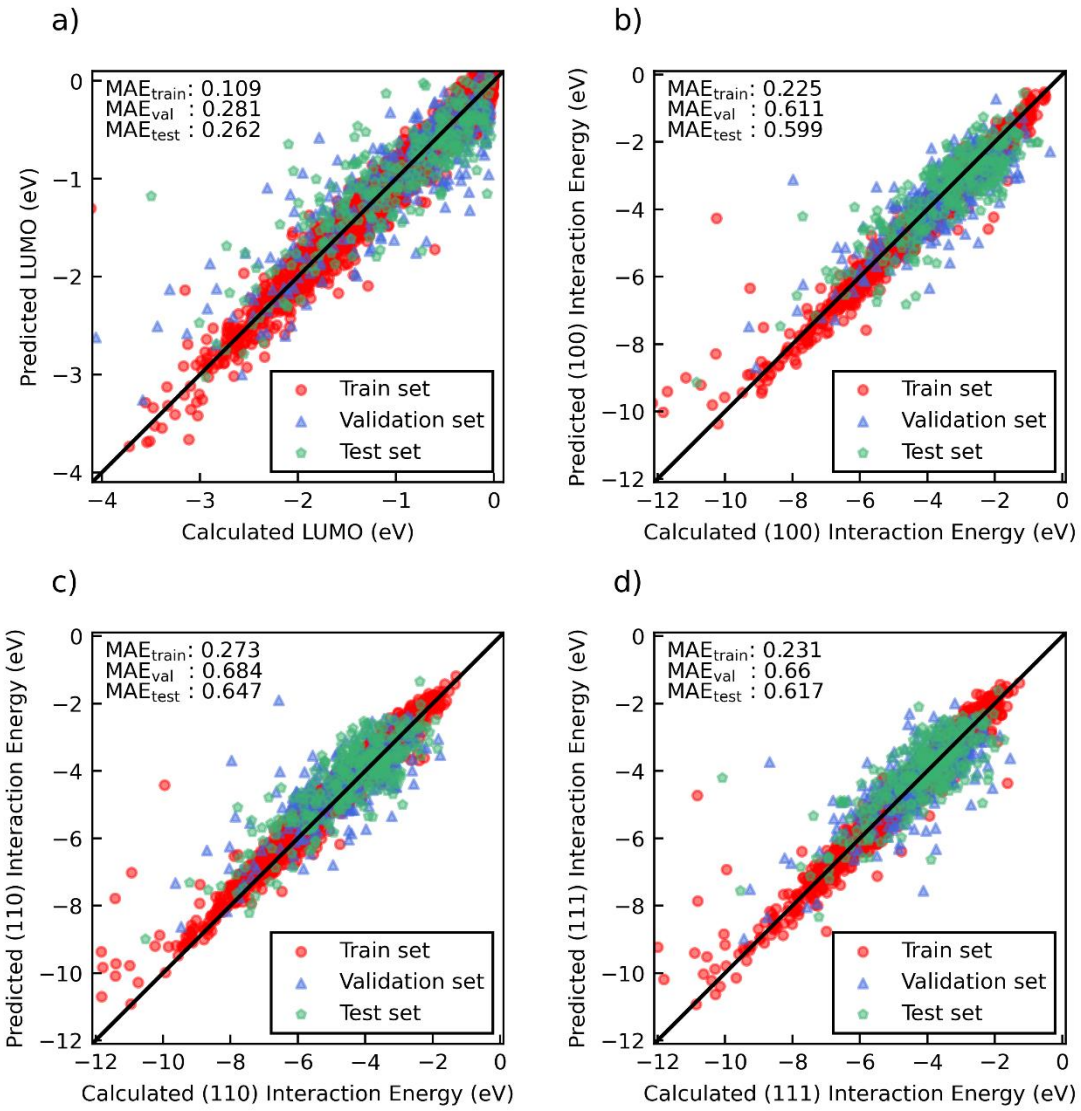


**Figure 2.** Parity plots from training of the initial surrogate SEI-model for a) LUMO energy (eV) from PubChemQC database, b) Interaction Energy on the (100) surface of Li metal (eV), c) Interaction Energy on the (110) surface of Li metal (eV), d) Interaction Energy on the (111) surface of Li metal (eV). The interaction energies were calculated using the M3GNet interatomic potential. The respective train, validation, and test set MAE (eV) of each of the objectives are shown on upper left corner of each plot.

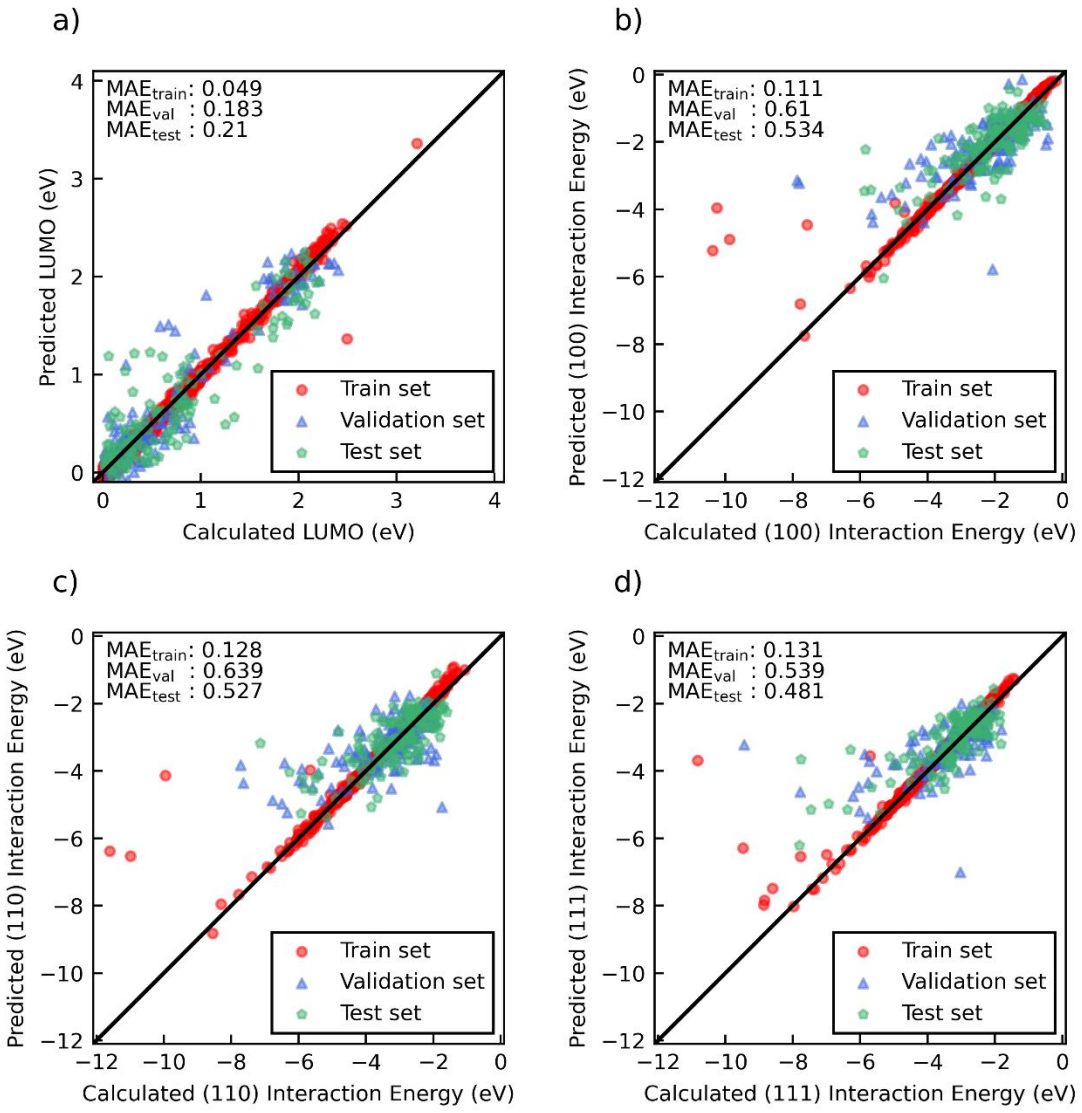


**Figure 3.** Parity plots from training of the initial surrogate LL-model for a) LUMO energy (eV) from PubChemQC database, b) Interaction Energy on the (100) surface of Li metal (eV), c) Interaction Energy on the (110) surface of Li metal (eV), d) Interaction Energy on the (111) surface of Li metal (eV). The interaction energies were calculated using the M3GNet interatomic potential. The respective train, validation, and test set MAE (eV) of each of the objectives are shown on upper left corner of each plot.

Bayesian Optimization seeks to obtain the global minimum of a black-box objective function using a sequential sampling approach by optimizing an acquisition function. Although numerous acquisition functions exist for single objective functions, there are limited options for multi-objective functions. Therefore, we perform scalarization in which a weighted sum of our optimization objectives was defined to combine our multiple objectives into a single objective function. This allows for the application of traditional single-objective BO techniques while ensuring weak Pareto optimality.[60–62] By assigning weights to each objective, the relative importance of each objective can be controlled, and the optimization problem can be transformed into a single-objective problem that seeks to minimize the weighted objective function.

We assigned an equal weight to the LUMO energy and the combined interaction energies (see Section S4 in Supporting Information). The aim is to minimize the weighted objective function, which leads to a low LUMO energy level and large (negative) interaction energies for SEI additives. In contrast, for LL additives, the LUMO energy level was maximized, along with the minimization of the interaction energies. The Expected Improvement (EI) acquisition function (see Section S4 in Supporting Information) was employed to recommend unlabeled molecules to be added to the dataset for the next iteration. These recommended molecules were subsequently labelled with their LUMO energy and M3GNet-calculated interaction energies. Thereafter, they were added to the training dataset and the surrogate model was retrained. This iterative cycle of recommending molecules followed by retraining of the surrogate model forms an active learning loop which persists until the entirety of the search space has been thoroughly screened. The BO process is illustrated in Figure 1 and is described in the Computational Methods section and Table S2 of the Supporting Information. To provide a consistent evaluation of the model's performance,

the same test set was used across all iterations (Figure 2). This active learning process was employed until the entire screening database was exhaustively explored.

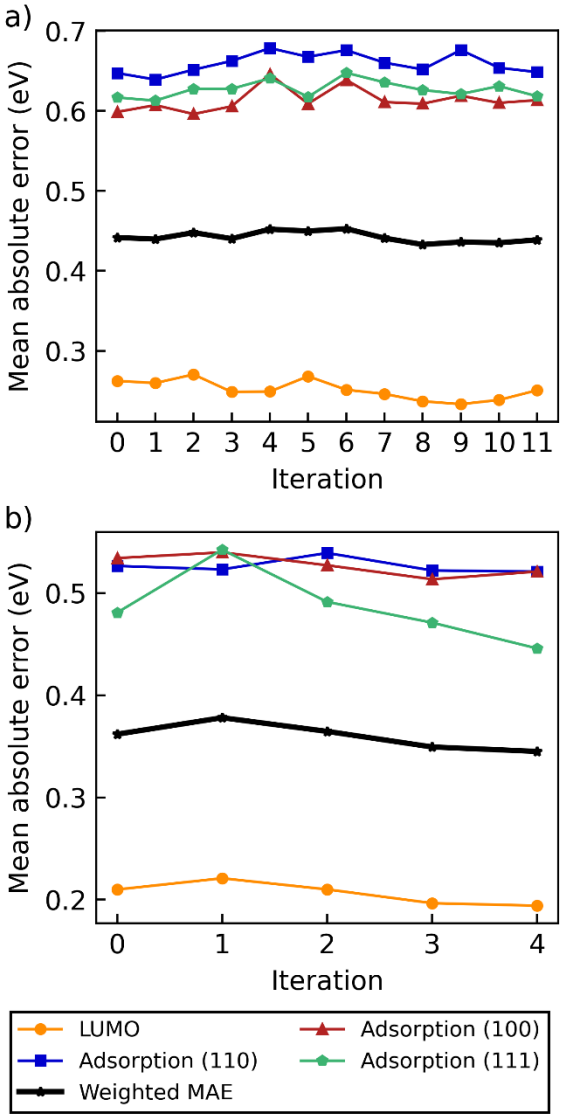


**Figure 3.** Evolution of test set MAE with each iteration of the Bayesian Optimization process for the a) SEI-model, b) LL-model. The same test set was used across all iterations. The weighted MAE is plotted as a function of the iterations, which is indicated by the black line. The weights used are identical to the weights of the optimization objective as defined in Section S4 of the Supporting Information.

**Discovery of promising additives**

To provide a benchmark for determining the effectiveness of a potential electrolyte additive, we performed the same calculations for 17 molecules (10 SEI additives, 3 LL additives, 4 additives using other mechanisms) that have been previously reported in the literature to be effective in suppressing the growth of Li dendrites (see Table S3 in Supporting Information). Our results show that the LL additives generally have a higher LUMO energy than SEI additives, which supports our conclusion that LL additives should aim to have a higher LUMO energy level.

After the Bayesian Optimization (BO) processes was completed, the final labeled dataset for the SEI additives comprised 160 molecules with scores surpassing the best score among the 10 reported SEI additives (CID: 24386, score: -9.65). The lowest score obtained was -22.21 (CID: 21797981), which is a weighted average of the LUMO energy and the interaction energies (see Section S4 in Supporting Information). However, not all these molecules are expected to be stable under standard conditions. To evaluate their stability, we calculated the DFT formation energy of these 160 molecules. Upon analysis, it was found that 146 out of the 160 molecules exhibited a negative formation energy. The negative value of the formation energy suggests that these molecules can be synthesized under normal conditions and remain stable. These findings indicate that these molecules show promise to be used as an electrolyte additive for suppressing the formation of Li dendrites in Li-metal batteries through the formation of a robust SEI layer.

For the LL additives, the final labeled dataset comprised of 801 molecules with scores surpassing the best score among the 3 reported LL-additives (CID: 2724563, score: -2.32). However, analysis of the final molecule-adsorbed structure revealed that a large number of these molecules are dissociated on the surface of the Li metal, indicating that the adsorption is irreversible. This is prevalent in most of the top scoring molecules, which produced large values

of interaction energies due to the formation of new compounds on the surface of Li. Therefore, we performed further screening to identify molecules which are not dissociated on the Li surface after adsorption. This is done by identifying the covalent bonds present on the molecule before and after adsorption. Molecules retaining an identical count of covalent bonds after adsorption are considered as likely to adsorb reversibly on the surface of Li. This subset is thus reduced to 13 molecules which are not dissociated after adsorption.

Importantly, the identification of potential dendrite-suppressing additives is rooted in the criterion in which the optimization score of potential molecules must surpass those of the reported additives. Relaxation of this criterion to identify potential additives could potentially encompass a broader spectrum of molecules, even those with lower scores, which may still hold significant potential for mitigating Li dendrite formation.

## Discussion

### Performance of surrogate model

To provide a visualization of the active learning process, the t-Distributed Stochastic Neighbor Embedding (t-SNE)[63] method was used to project the multi-dimensional molecular fingerprint into two dimensions (Figure 4). t-SNE is a nonlinear dimensionality reduction technique which measures the pairwise similarity between high-dimensional data points and between their low-dimensional counterparts. It minimizes the Kullback-Leibler (KL) divergence between the joint probability distributions in the high-dimensional space and the low-dimensional space, thereby preserving the local and global relationships among the data points.

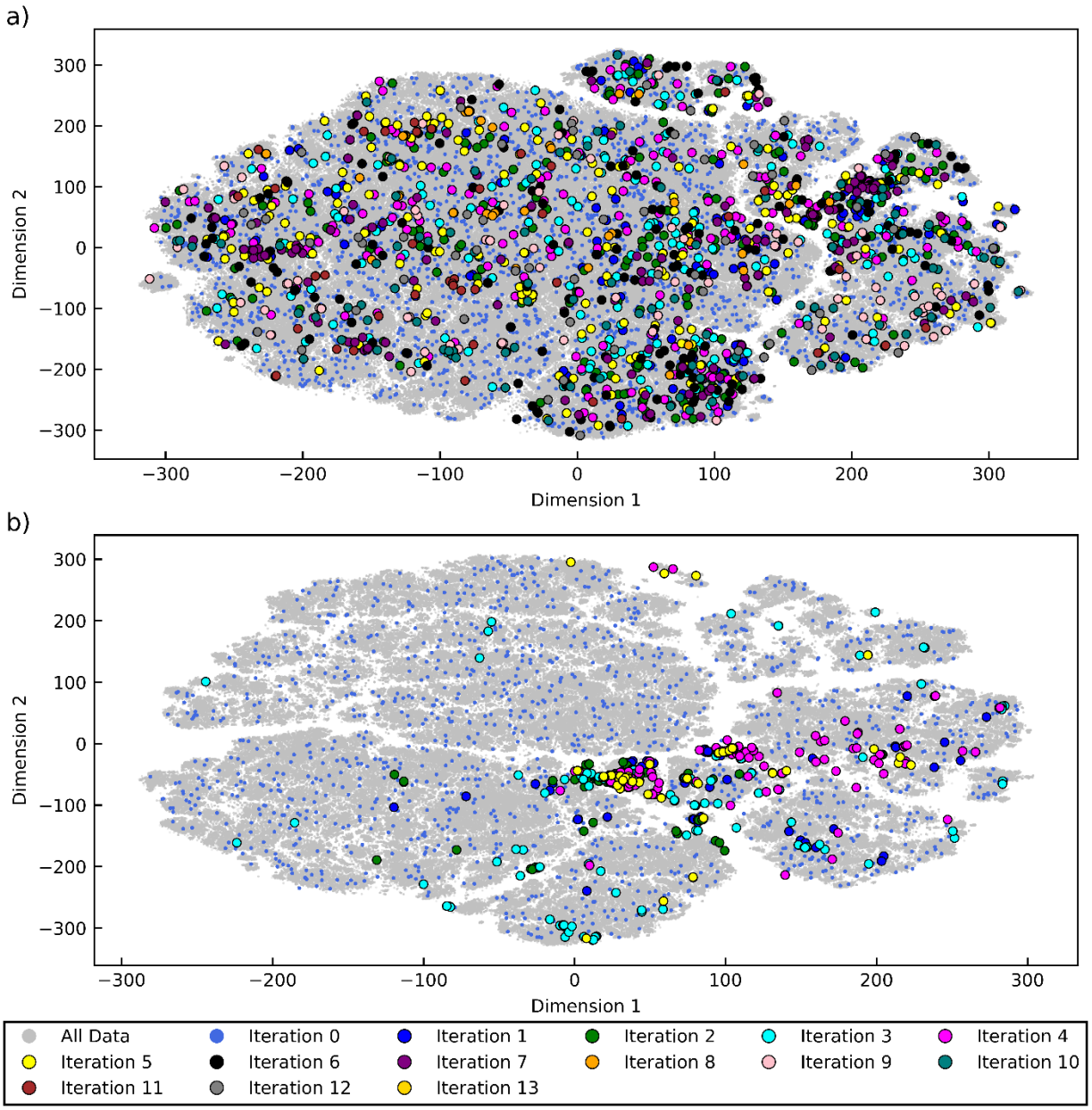


**Figure 4.** t-Distributed Stochastic Neighbor Embedding (t-SNE) plot of the search space and Bayesian Optimization process for the a) SEI additives, and b) LL additives. The t-SNE algorithm was implemented using the scikit-learn package.[64] A perplexity value of 100 was used and the algorithm ran for 5000 iterations. The final KL divergence obtained was 3.712 and 2.664 for the SEI-search space and LL-search space respectively.

Figure 4 illustrates that the initial training data is evenly distributed across the entire search spaces, indicating that our randomly selected molecules can efficiently fill the search space. This ensures the robustness of the initial surrogate model and its ability to generalize effectively. It can be observed that in the earlier iterations (1 to 3), the recommended molecules form distinct clusters, with a few molecules located far away from these clusters. This pattern demonstrates a favorable trade-off between exploration and exploitation. Furthermore, the proposed molecules are distributed throughout the entire design space across all iterations of Bayesian Optimization. This distribution indicates that our BO strategy can discover potential molecules that are dissimilar to each other with the desired properties, thereby ensuring our model's capability to make accurate predictions across the molecular design space.

From Figures 2, 3 and 4, we observe that the MAE of the predicted LUMO energy is consistently the lowest compared to the interaction energies. At the final iteration, the weighted MAE decreases to 0.439 eV and 0.345 eV for the SEI model and LL model respectively (Figure 4), showing the efficacy of the self-improving active learning process where the model improves its accuracy through the optimization of the weighted objective function. From Figure 4, it can be observed that the MAE of the LUMO energy had a more significant decrease than the MAE of the interaction energies. Since adsorption of complex molecules is a complicated process, accurately predicting the highest interaction energy is expected to be a difficult task. The surface energies of metals are also not accurately modelled using high-accuracy DFT methods, yielding inadequate accuracies with commonly employed DFT functionals.[65] A benchmark of various DFT functionals on an adsorption dataset consisting of simple molecules yielded errors of 0.13-0.93 eV (0.015-0.32 eV/atom) with respect to experimental results for adsorption energies on transition metal surfaces using various common functionals,[66] which shows that even high accuracy first-principles

calculations are unable to accurately model the adsorption of molecules on the surface of metals. Since the interaction energies in our data are obtained using the M3GNet potential, errors arising from the use of ML potentials are expected to be propagated to the surrogate model as well. Additionally, it has also been suggested that graph-based models are not able to accurately capture non-local effects such as dispersion, resulting in reduced accuracy for the prediction of adsorption energies using graph-based methods.[44] Despite the difficulty of predicting accurate interaction energies, the test set MAE of interaction energies for the initial surrogates are 0.62 eV (0.024 eV/atom) for the SEI-model and 0.51 eV (0.018 eV/atom) for the LL-model, which is well within range of DFT calculations. Therefore, it is unlikely that the error in our predictions can be further improved from repeated trainings of the models. It is worth noting that the accuracy of the surrogate model does not largely affect the search process. Empirical observations have shown that a highly accurate machine learning model is not always a prerequisite for accelerating the search process when active learning is integrated, specifically in situations where the recommendation of the next experiment or computation is involved.[67]

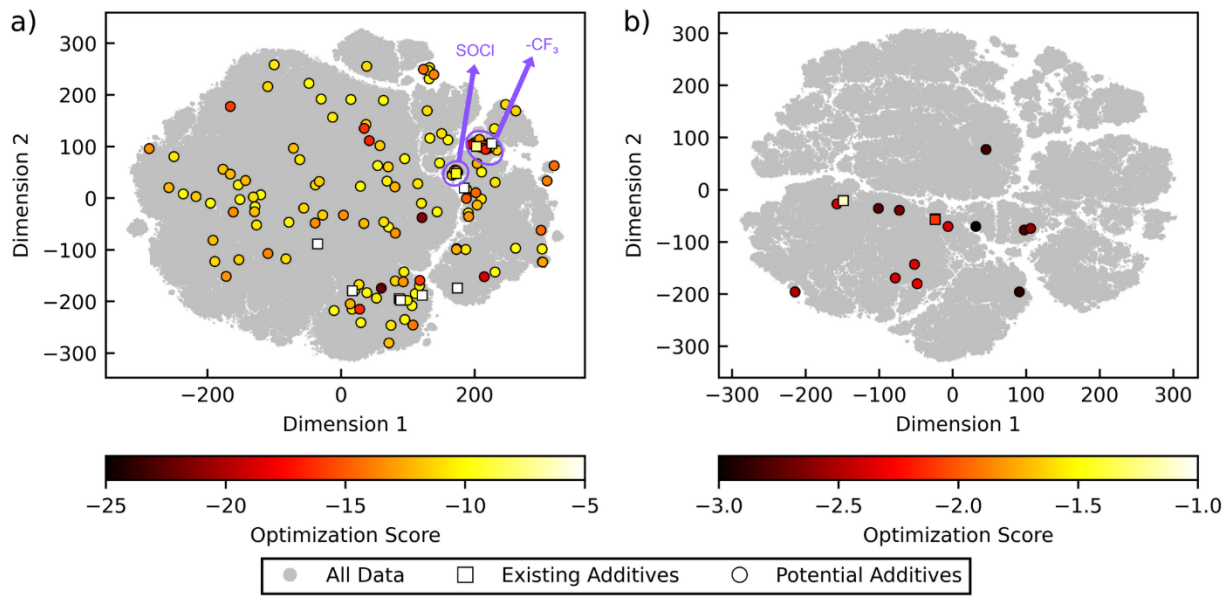


**Figure 5.** t-SNE plot showing the existing additives reported in literature and the additives predicted with superior performance for the a) SEI additives, and b) LL additives. The squares represent the existing additives while the circles represent the potential additives. The heatmap indicates the optimization score obtained from the BO process. A lower optimization score indicates a higher performance (more ideal design parameters).

**Characteristics of novel electrolyte additives**

The optimization of the search space to screen for SEI-additives yielded potential molecules with a low LUMO energy level and high interaction energies on the Li surfaces. We have set a criterion on the optimization score whereby molecules with a better score than the best scoring molecules reported in literature are predicted to have superior performance as a SEI-additive, which consists of a set of 146 molecules with negative formation energies. From Figure 5a, we observe distinct clusters of potential molecules located in proximity to specific existing additives. These areas are representative of certain features such as thionyl chloride groups (SOCl) and highly fluorinated molecules (-$CF_3$), which may serve as design principles. Notably, many

potential additives are also dispersed far away from the existing additives, which suggests that there are new design spaces to be explored. Upon analysis of the final molecule-adsorbed structure of these set of molecules, it is observed that all of them undergo dissociative adsorption (chemisorption) on the Li surface to form several products, indicating that our optimization process had successfully screened potential molecules which are able to form SEI layers with relative ease. The ease of dissociative adsorption may be explained as due to many of these molecules having relatively unstable bonds (O-F, N-F, O-O) which have low bond energies and thus easy to break, leading to extremely large values of interaction energies due to the formation of more stable compounds on the Li surface. As such, these molecules undergo dissociative adsorption easily on the Li surface to form $Li_2O$, LiF and $Li_3N$ compounds, which are seen in the final molecule-adsorbed structures. It is well known that LiF plays an important role in forming dense and stable SEI layers.[25,32,68,69] Indeed, among these set of molecules, 79% contain fluorine, highlighting the importance of fluorinated additives for forming robust SEI layers.

For the LL-additives, large interaction energies are preferred but the molecule needs to be stable (i.e., not dissociated on the Li surface). From the results of our BO process, 13 molecules are expected to have superior performance as a LL additive, which are able to undergo non-dissociative adsorption. The levelling mechanism can be explained by a reduced energy barrier for Li deposition and surface diffusion when the molecule is adsorbed on the Li surface, enabling a smooth plating of Li ions.[40,41] Structural similarities in these 13 molecules consists of carbonyl groups (C=O) and amine (R-N) groups present on organic molecules (>3 carbon atoms). From Figure 5b, it is observed that one potential additive ($C_6H_{10}N_2O_2$) is in proximity with an existing additive ($C_6H_9NO$) where similar features between these two molecules include a lactam ring. Primarily, there is no clear set of design principles for the features of LL additives, as seen in

Figure 5b where potential additives are scattered away from each other. Analysis of the molecule-adsorbed structure revealed that the most favorable adsorption occurs when the heteroatoms are adsorbed on the hollow and bridge sites of the Li surface. For reversible adsorption to occur, heteroatoms can increase the binding affinity of the additive to the Li surface, but the affinity should not be too strong such that the molecule adsorbs irreversibly and dissociates. These heteroatoms may serve as nucleation sites for ease of Li deposition and facilitating the levelling effect. We postulate that there is an optimal adsorption energy in which the levelling effect is maximized, following the Sabatier principle. In contrast to SEI-additives, fluorine is not preferred on these additives, due to their tendency to form LiF from dissociative adsorption.

We note that only charge neutral molecules are considered in this study although ionic compounds had been reported to suppress dendrite formation through other mechanisms.[27,70,71] We have not included any charged molecules in our search space since electrostatic effects on the interaction energy are not well modelled using current computational methods.

**Accuracy of Interatomic Potential**

In order to verify the accuracy of the M3GNet interatomic potential, we performed DFT-D3 calculations for 112 of the top SEI-additives obtained from the optimization process and the 17 previously reported additives in literature. The same initial starting molecule-adsorbed structure was used for the DFT-D3 calculations to ensure accurate comparisons between the calculations. The details of our DFT calculations can be found in the Computational Methods section.

To ensure that the computations remain tractable, only the interaction energy of the molecule on the (100) surface of Li was considered. The interaction energy obtained from DFT was then compared against the corresponding values derived from the M3GNet interatomic

potential (as illustrated in Figure 6). The MAE of the M3GNet-computed interaction energy and the DFT-computed interaction energy is 0.37 eV/atom for the (100) surface. From Figure 6, it can be observed that the interaction energy calculated from DFT-D3 is consistently larger than the energy calculated using M3GNet. This observation can be attributed to the D3 correction scheme,[72] which includes dispersion effects that the M3GNet interatomic potential is unable to reproduce. Despite so, the M3GNet error is within the range of adsorption energy errors predicted by DFT.[66] Most importantly, it can be seen from Figure 6 that our optimization process is able to recommend molecules with larger interaction energies than existing additives, regardless of whether it is calculated using the M3GNet interatomic potential or DFT. This indicates that the use of the M3GNet interatomic potential provides sufficient accuracy for screening purposes.

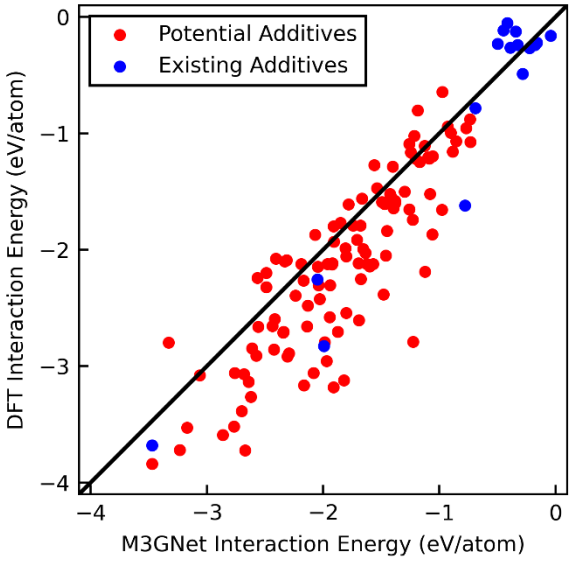


**Figure 6.** Parity plots for the M3GNet-computed interaction energy (eV/atom) calculated on the (100) surface of Li metal versus the DFT-computed interaction energy. The red circles represent the potential additives from optimization while the blue circles represent the existing additives reported in literature.

## Conclusion

We investigated potential electrolyte additives as a means of mitigating Li dendrite formation within Li-metal batteries, employing an inverse design strategy. By investigating the underlying mechanisms that contribute to dendrite suppression – namely, the formation of robust solid electrolyte interphase (SEI) layers and the levelling mechanism – we have strategically oriented our design approach towards key molecular descriptors, including the LUMO energy and the interaction energy upon Li surface adsorption. To minimize computational cost, an active learning process based on Bayesian Optimization was proposed to identify promising molecules which can satisfy the criterion to act as effective additives. Our BO process identified 146 molecules which can act as a SEI-forming additive and 13 molecules which can act as a leveller additive, expected to outperform existing additives reported in literature. These molecules are suggested for experimental validation to determine their efficacy in dendrite suppression. Although our current search space was confined to the PubChemQC database, it can be extended to a larger search space to screen for more potential additives. As databases expand and computational power improves, it is with hope that our framework yields important insights into the accelerated discovery of electrolyte additives for Li-metal batteries.

## Computational Details

### Interaction Energy calculations

Starting from a given geometry of the molecule, we perform rotations along the x- and y-axes at intervals of 15˚ to generate different initial geometries of the molecule. To keep the number of computations tractable, we only consider the top ten geometries which give the lowest average

distance of all atoms from the slab surface. These geometries are expected to possess the highest interaction with the surface, hence are more likely to have a higher interaction energy. Each geometry of the molecule was placed on the low-index facets of the Li surface: (100), (110), (111) surfaces, on different adsorption sites enumerated by the Python Materials Genomics (pymatgen) package.[73] A vacuum size of 20Å and four atomic layers were used for all surfaces. The dimensions of the surface were appropriately scaled according to the length of the molecule to minimize coverage effects.

The Interaction Energy ($E_{interaction}$) is calculated using Equation (1):

$$E_{interaction} = E_{surface+adsorbate} - (E_{surface} + E_{adsorbate}) \quad (1)$$

where $E_{surface+adsorbate}$ is the total energy of the Li surface with the adsorbate, $E_{surface}$ and $E_{adsorbate}$ are the total energies of the pristine Li surface and the adsorbate in the gas phase respectively. The total energies of all systems were obtained after relaxation using the M3GNet interatomic potential. Each molecule was labeled with its LUMO energy from the PubChemQC database, as well as the highest (most negative) interaction energies obtained from M3GNet relaxations on each surface across all initial configurations of the molecule.

**Molecular Graph Convolutional Neural Network**

Each molecule can be defined as an undirected graph $G = (V, E)$ where each vertex ($V$) represents a single atom, and each edge ($E$) represents a bond between neighboring atoms. The vertices carry atomic information such as atomic number, electronegativity, hybridization, and other relevant features. A total of 75 atomic features were encoded in each vertex. In each graph convolution layer of the molecular graph convolutional neural network, the atomic features at every vertex will be updated with information from the neighboring vertices and itself. This process enables the learning of a graph convolutional weight parameter matrix, facilitating the

optimal exchange of information to encode the most representative features of the molecule. Through multiple iterations of information exchange via the convolutional layers, the processed hidden features at each vertex are then gathered using a graph gathering layer, resulting in the formation of the final molecular fingerprint.[59] The molecular fingerprint is then passed through several fully connected layers to produce the final predictions of the LUMO energy and minimum interaction energies of each molecule. All weight parameters in the graph convolutional layers and fully connected layers were trained and updated by gradient descent methods. The model was implemented using a modified version from the deepchem package[74] in Python and used as the surrogate model for Bayesian Optimization. To prevent overfitting, for all iterations, early stopping was implemented whereby the best weights that produced the lowest MAE on the validation set from all epochs were used as the final model.

**Bayesian Optimization**

To screen the entire space, the unlabeled datasets were first divided into smaller subsets of ~100,000 molecules each. Molecules which failed the featurization by the surrogate model were removed from the dataset. During each iteration of the BO process, the surrogate model predicts each target variable and their corresponding uncertainty. The uncertainty in the predictions was obtained using the Monte Carlo dropout method whereby different dropout masks were employed in the model, allowing an estimate of the aleatoric and epistemic uncertainty in the predictions.[75] The weighted optimization objective was then calculated and the Expected Improvement (EI) acquisition function ranks the molecules in terms of their EI score. The top 200 molecules with the best EI score were then chosen to perform interaction energy calculations to obtain new labelled data to be added into the database (see Table S2 in Supporting Information). The number of recommendations were decided by the time required to perform interaction energy calculations

(~3 days). Subsequently, the surrogate models were retrained with the newly added data. The performance of the surrogate models was evaluated on a fixed test set of 287 and 140 molecules for the SEI-model and LL-model respectively across each iteration of the BO process.

**DFT calculations**

The Vienna Ab initio Simulation Package (VASP)[76,77] was used to perform DFT-D3 calculations for the verification of the interaction energy on the (100) surface of Li metal with the M3GNet interatomic potential. The spin-polarized generalized gradient approximation (GGA)-type Perdew–Burke–Ernzerhof (PBE) functional was used to approximate the unknown exchange-correlation contribution in DFT.[78] Additionally, the D3-correction scheme was applied to include dispersion effects of the adsorbate on the surface of the Li metal.[72] The projected augmented wave (PAW) potentials were used for the description of core electrons.[79] Valence electrons were represented using plane waves up to an energy cutoff of 520 eV. A Γ-centered Monkhorst-Pack k-point mesh with 25 subdivisions along each reciprocal lattice vector was used for all structures.[80] The total energy of each structure was converged to within $10^{-5}$ eV/cell, and atomic forces within $10^{-2}$ eV/Å. The initial starting structures used were identical to the structures which produced the minimum interaction energy during M3GNet relaxation. Finally, the interaction energy was calculated using Equation (1).

## Associated content

The Supporting Information contains:

1) The lists of labelled molecules for SEI-additives and LL-additives (CSV) after the final iteration of Bayesian Optimization, which consists of their LUMO energy and M3GNet calculated interaction energies on the (100), (110) and (111) surfaces of Li metal. The molecules can be identified by their CID number and SMILES string. The molecules are sorted based on their optimization score (potential SEI additives are at the top 146 entries, potential LL additives are at the top 13 entries).

2) Supporting Information (PDF) which consists of details of our Bayesian Optimization process, model hyperparameters, model comparisons and a list of previously reported electrolyte additives in the literature.

## Corresponding Author

*E-mail: ngmf@ihpc.a-star.edu.sg

## ORCID

Damien K. J. Lee: 0009-0006-1100-6477

Teck Leong Tan: 0000-0002-7089-8966

Man-Fai Ng: 0000-0001-7696-2706

## Notes

The authors declare no competing financial interest.

The source codes used in this study can be found in the following GitHub repository: https://github.com/damienlkj/screening_electrolyte_additives .

## Acknowledgments

We acknowledge the National Supercomputing Center (NSCC) Singapore, the High Performance Computing (HPC) resources at the National University of Singapore and the A*STAR Computational Resource Centre (A*CRC) of Singapore for the use of its high-performance computing facilities. TLT acknowledges support from the Singapore National Research Foundation's Competitive Research Program funding (NRF-CRP23-2019-0001).

## References

(1) Xu, W.; Wang, J.; Ding, F.; Chen, X.; Nasybulin, E.; Zhang, Y.; Zhang, J.-G. Lithium Metal Anodes for Rechargeable Batteries. *Energy Environ. Sci.* **2014**, *7* (2), 513–537. https://doi.org/10.1039/C3EE40795K.

(2) Wang, R.; Cui, W.; Chu, F.; Wu, F. Lithium Metal Anodes: Present and Future. *J. Energy Chem.* **2020**, *48*, 145–159. https://doi.org/10.1016/j.jechem.2019.12.024.

(3) Liu, B.; Zhang, J.-G.; Xu, W. Advancing Lithium Metal Batteries. *Joule* **2018**, *2* (5), 833–845. https://doi.org/10.1016/j.joule.2018.03.008.

(4) Whittingham, M. S. Electrical Energy Storage and Intercalation Chemistry. *Science* **1976**, *192* (4244), 1126–1127. https://doi.org/10.1126/science.192.4244.1126.

(5) Xiao, J. How Lithium Dendrites Form in Liquid Batteries. *Science* **2019**, *366* (6464), 426–427. https://doi.org/10.1126/science.aay8672.

(6) Fan, X.; Chen, L.; Borodin, O.; Ji, X.; Chen, J.; Hou, S.; Deng, T.; Zheng, J.; Yang, C.; Liou, S.-C.; Amine, K.; Xu, K.; Wang, C. Non-Flammable Electrolyte Enables Li-Metal Batteries with Aggressive Cathode Chemistries. *Nat. Nanotechnol.* **2018**, *13* (8), 715–722. https://doi.org/10.1038/s41565-018-0183-2.

(7) Nagaura, T.; Tozawa, K. Lithium Ion Rechargeable Battery. *Prog. Batter. Sol. Cells* **1990**, *9* (209).

(8) Li, M.; Lu, J.; Chen, Z.; Amine, K. 30 Years of Lithium-Ion Batteries. *Adv. Mater.* **2018**, *30* (33), 1800561. https://doi.org/10.1002/adma.201800561.

(9) Cheng, X.-B.; Zhang, R.; Zhao, C.-Z.; Zhang, Q. Toward Safe Lithium Metal Anode in Rechargeable Batteries: A Review. *Chem. Rev.* **2017**, *117* (15), 10403–10473. https://doi.org/10.1021/acs.chemrev.7b00115.

(10) Han, X.; Gong, Y.; Fu, K. (Kelvin); He, X.; Hitz, G. T.; Dai, J.; Pearse, A.; Liu, B.; Wang, H.; Rubloff, G.; Mo, Y.; Thangadurai, V.; Wachsman, E. D.; Hu, L. Negating Interfacial Impedance in Garnet-Based Solid-State Li Metal Batteries. *Nat. Mater.* **2017**, *16* (5), 572–579. https://doi.org/10.1038/nmat4821.

(11) Fu, K. (Kelvin); Gong, Y.; Liu, B.; Zhu, Y.; Xu, S.; Yao, Y.; Luo, W.; Wang, C.; Lacey, S. D.; Dai, J.; Chen, Y.; Mo, Y.; Wachsman, E.; Hu, L. Toward Garnet Electrolyte–Based Li Metal Batteries: An Ultrathin, Highly Effective, Artificial Solid-State Electrolyte/Metallic Li Interface. *Sci. Adv.* **2017**, *3* (4), e1601659. https://doi.org/10.1126/sciadv.1601659.

(12) Cheng, X.-B.; Zhao, C.-Z.; Yao, Y.-X.; Liu, H.; Zhang, Q. Recent Advances in Energy Chemistry between Solid-State Electrolyte and Safe Lithium-Metal Anodes. *Chem* **2019**, *5* (1), 74–96. https://doi.org/10.1016/j.chempr.2018.12.002.

(13) Park, S.; Jin, H.-J.; Yun, Y. S. Advances in the Design of 3D-Structured Electrode Materials for Lithium-Metal Anodes. *Adv. Mater.* **2020**, *32* (51), 2002193. https://doi.org/10.1002/adma.202002193.
(14) Tu, Z.; Kambe, Y.; Lu, Y.; Archer, L. A. Nanoporous Polymer-Ceramic Composite Electrolytes for Lithium Metal Batteries. *Adv. Energy Mater.* **2014**, *4* (2), 1300654. https://doi.org/10.1002/aenm.201300654.
(15) Liu, J.; Bao, Z.; Cui, Y.; Dufek, E. J.; Goodenough, J. B.; Khalifah, P.; Li, Q.; Liaw, B. Y.; Liu, P.; Manthiram, A.; Meng, Y. S.; Subramanian, V. R.; Toney, M. F.; Viswanathan, V. V.; Whittingham, M. S.; Xiao, J.; Xu, W.; Yang, J.; Yang, X.-Q.; Zhang, J.-G. Pathways for Practical High-Energy Long-Cycling Lithium Metal Batteries. *Nat. Energy* **2019**, *4* (3), 180–186. https://doi.org/10.1038/s41560-019-0338-x.
(16) Haregewoin, A. M.; Wotango, A. S.; Hwang, B.-J. Electrolyte Additives for Lithium Ion Battery Electrodes: Progress and Perspectives. *Energy Env. Sci* **2016**, *9* (6), 1955–1988. https://doi.org/10.1039/C6EE00123H.
(17) Zhang, S. S. A Review on Electrolyte Additives for Lithium-Ion Batteries. *J. Power Sources* **2006**, *162* (2), 1379–1394. https://doi.org/10.1016/j.jpowsour.2006.07.074.
(18) Zhang, H.; Eshetu, G. G.; Judez, X.; Li, C.; Rodriguez-Martínez, L. M.; Armand, M. Electrolyte Additives for Lithium Metal Anodes and Rechargeable Lithium Metal Batteries: Progress and Perspectives. *Angew. Chem. Int. Ed.* **2018**, *57* (46), 15002–15027. https://doi.org/10.1002/anie.201712702.
(19) Ye, S.; Wang, L.; Liu, F.; Shi, P.; Wang, H.; Wu, X.; Yu, Y. G-C3N4 Derivative Artificial Organic/Inorganic Composite Solid Electrolyte Interphase Layer for Stable Lithium Metal Anode. *Adv. Energy Mater.* **2020**, *10* (44), 2002647. https://doi.org/10.1002/aenm.202002647.
(20) Zhai, P.; Wang, T.; Jiang, H.; Wan, J.; Wei, Y.; Wang, L.; Liu, W.; Chen, Q.; Yang, W.; Cui, Y.; Gong, Y. 3D Artificial Solid-Electrolyte Interphase for Lithium Metal Anodes Enabled by Insulator–Metal–Insulator Layered Heterostructures. *Adv. Mater.* **2021**, *33* (13), 2006247. https://doi.org/10.1002/adma.202006247.
(21) Lee, S. H.; Hwang, J.-Y.; Park, S.-J.; Park, G.-T.; Sun, Y.-K. Adiponitrile (C6H8N2): A New Bi-Functional Additive for High-Performance Li-Metal Batteries. *Adv. Funct. Mater.* **2019**, *29* (30), 1902496. https://doi.org/10.1002/adfm.201902496.
(22) Lei, Y.; Xie, Y.; Huang, Y.; Wang, Q.; Li, Z.; Wu, X.; Qiao, Y.; Dai, P.; Huang, L.; Hua, Y.; Wang, C.; Sun, S. Amidinothiourea as a New Deposition-Regulating Additive for Dendrite-Free Lithium Metal Anodes. *Chem. Commun.* **2021**, *57* (78), 10055–10058. https://doi.org/10.1039/D1CC02829D.
(23) Park, S.-J.; Hwang, J.-Y.; Sun, Y.-K. Trimethylsilyl Azide (C3H9N3Si): A Highly Efficient Additive for Tailoring Fluoroethylene Carbonate (FEC) Based Electrolytes for Li-Metal Batteries. *J. Mater. Chem. A* **2019**, *7* (22), 13441–13448. https://doi.org/10.1039/C9TA03713F.
(24) Li, S.; Dai, H.; Li, Y.; Lai, C.; Wang, J.; Huo, F.; Wang, C. Designing Li-Protective Layer via SOCl2 Additive for Stabilizing Lithium-Sulfur Battery. *Energy Storage Mater.* **2019**, *18*, 222–228. https://doi.org/10.1016/j.ensm.2018.09.012.
(25) Markevich, E.; Salitra, G.; Aurbach, D. Fluoroethylene Carbonate as an Important Component for the Formation of an Effective Solid Electrolyte Interphase on Anodes and Cathodes for Advanced Li-Ion Batteries. *ACS Energy Lett.* **2017**, *2* (6), 1337–1345. https://doi.org/10.1021/acsenergylett.7b00163.

(26) Jeong, J.; Lee, J.-N.; Park, J.-K.; Ryou, M.-H.; Lee, Y. M. Stabilizing Effect of 2-(Triphenylphosphoranylidene) Succinic Anhydride as Electrolyte Additive on the Lithium Metal of Lithium Metal Secondary Batteries. *Electrochimica Acta* **2015**, *170*, 353–359. https://doi.org/10.1016/j.electacta.2015.04.168.
(27) Liu, S.; Li, G.-R.; Gao, X.-P. Lanthanum Nitrate As Electrolyte Additive To Stabilize the Surface Morphology of Lithium Anode for Lithium–Sulfur Battery. *ACS Appl. Mater. Interfaces* **2016**, *8* (12), 7783–7789. https://doi.org/10.1021/acsami.5b12231.
(28) Ding, F.; Xu, W.; Graff, G. L.; Zhang, J.; Sushko, M. L.; Chen, X.; Shao, Y.; Engelhard, M. H.; Nie, Z.; Xiao, J.; Liu, X.; Sushko, P. V.; Liu, J.; Zhang, J.-G. Dendrite-Free Lithium Deposition via Self-Healing Electrostatic Shield Mechanism. *J. Am. Chem. Soc.* **2013**, *135* (11), 4450–4456. https://doi.org/10.1021/ja312241y.
(29) Miao, R.; Yang, J.; Feng, X.; Jia, H.; Wang, J.; Nuli, Y. Novel Dual-Salts Electrolyte Solution for Dendrite-Free Lithium-Metal Based Rechargeable Batteries with High Cycle Reversibility. *J. Power Sources* **2014**, *271*, 291–297. https://doi.org/10.1016/j.jpowsour.2014.08.011.
(30) Monroe, C.; Newman, J. The Impact of Elastic Deformation on Deposition Kinetics at Lithium/Polymer Interfaces. *J. Electrochem. Soc.* **2005**, *152* (2), A396. https://doi.org/10.1149/1.1850854.
(31) Xu, K. Electrolytes and Interphases in Li-Ion Batteries and Beyond. *Chem. Rev.* **2014**, *114* (23), 11503–11618. https://doi.org/10.1021/cr500003w.
(32) Choudhury, S.; Archer, L. A. Lithium Fluoride Additives for Stable Cycling of Lithium Batteries at High Current Densities. *Adv. Electron. Mater.* **2016**, *2* (2), 1500246. https://doi.org/10.1002/aelm.201500246.
(33) Han, G.-B.; Lee, J.-N.; Lee, D. J.; Lee, H.; Song, J.; Lee, H.; Ryou, M.-H.; Park, J.-K.; Lee, Y. M. Enhanced Cycling Performance of Lithium Metal Secondary Batteries with Succinic Anhydride as an Electrolyte Additive. *Electrochimica Acta* **2014**, *115*, 525–530. https://doi.org/10.1016/j.electacta.2013.11.015.
(34) Fu, X.; Wang, G.; Dang, D.; Liu, Q.; Xiong, X.; Wu, C. Sulfuryl Chloride as a Functional Additive towards Dendrite-Free and Long-Life Li Metal Anodes. *J. Mater. Chem. A* **2019**, *7* (43), 25003–25009. https://doi.org/10.1039/C9TA09068A.
(35) Yang, S.; Hao, M.; Wang, Z.; Xie, Z.; Cai, Z.; Hu, M.; Chen, B.; Wang, L.; Zhou, K. 2,2,2-Trifluoroethyl Trifluoroacetate as Effective Electrolyte Additive for Uniform Li Deposition in Lithium Metal Batteries. *Chem. Eng. J.* **2022**, *435*, 134897. https://doi.org/10.1016/j.cej.2022.134897.
(36) Wang, X.; Mai, W.; Guan, X.; Liu, Q.; Tu, W.; Li, W.; Kang, F.; Li, B. Recent Advances of Electroplating Additives Enabling Lithium Metal Anodes to Applicable Battery Techniques. *Energy Environ. Mater.* **2021**, *4* (3), 284–292. https://doi.org/10.1002/eem2.12109.
(37) Lai, Z.; Wang, S.; Wang, C.; Hong, Y.; Zhou, G.; Chen, Y.; He, W.; Peng, Y.; Xiao, D. A Comparison of Typical Additives for Copper Electroplating Based on Theoretical Computation. *Comput. Mater. Sci.* **2018**, *147*, 95–102. https://doi.org/10.1016/j.commatsci.2017.11.049.
(38) Dow, W.-P.; Yen, M.-Y.; Liao, S.-Z.; Chiu, Y.-D.; Huang, H.-C. Filling Mechanism in Microvia Metallization by Copper Electroplating. *Electrochimica Acta* **2008**, *53* (28), 8228–8237. https://doi.org/10.1016/j.electacta.2008.06.042.

(39) Moffat, T. P.; Wheeler, D.; Kim, S.-K.; Josell, D. Curvature Enhanced Adsorbate Coverage Mechanism for Bottom-up Superfilling and Bump Control in Damascene Processing. *Electrochimica Acta* **2007**, *53* (1), 145–154. https://doi.org/10.1016/j.electacta.2007.03.025.
(40) Wang, Q.; Yang, C.; Yang, J.; Wu, K.; Hu, C.; Lu, J.; Liu, W.; Sun, X.; Qiu, J.; Zhou, H. Dendrite-Free Lithium Deposition via a Superfilling Mechanism for High-Performance Li-Metal Batteries. *Adv. Mater.* **2019**, *31* (41), 1903248. https://doi.org/10.1002/adma.201903248.
(41) Lee, J.-S.; Shin, K.; Jun, S.-Y.; Kim, S.; Ryu, W.-H. Dual-Functional Vinylpyrrolidone Electrolyte Additive as Anode Surface Leveler and Cathode Catalyst for Lithium Metal-Oxygen Batteries. *Chem. Eng. J.* **2023**, *458*, 141383. https://doi.org/10.1016/j.cej.2023.141383.
(42) Goodenough, J. B.; Kim, Y. Challenges for Rechargeable Li Batteries. *Chem. Mater.* **2010**, *22* (3), 587–603. https://doi.org/10.1021/cm901452z.
(43) Butler, K. T.; Davies, D. W.; Cartwright, H.; Isayev, O.; Walsh, A. Machine Learning for Molecular and Materials Science. *Nature* **2018**, *559* (7715), 547–555. https://doi.org/10.1038/s41586-018-0337-2.
(44) Pablo-García, S.; Morandi, S.; Vargas-Hernández, R. A.; Jorner, K.; Ivković, Ž.; López, N.; Aspuru-Guzik, A. Fast Evaluation of the Adsorption Energy of Organic Molecules on Metals via Graph Neural Networks. *Nat. Comput. Sci.* **2023**, *3* (5), 433–442. https://doi.org/10.1038/s43588-023-00437-y.
(45) Ng, M.-F.; Sun, Y.; Seh, Z. W. Machine Learning-Inspired Battery Material Innovation. *Energy Adv.* **2023**, *2* (4), 449–464. https://doi.org/10.1039/D3YA00040K.
(46) Ling, C. A Review of the Recent Progress in Battery Informatics. *Npj Comput. Mater.* **2022**, *8* (1), 1–22. https://doi.org/10.1038/s41524-022-00713-x.
(47) Lombardo, T.; Duquesnoy, M.; El-Bouysidy, H.; Årén, F.; Gallo-Bueno, A.; Jørgensen, P. B.; Bhowmik, A.; Demortière, A.; Ayerbe, E.; Alcaide, F.; Reynaud, M.; Carrasco, J.; Grimaud, A.; Zhang, C.; Vegge, T.; Johansson, P.; Franco, A. A. Artificial Intelligence Applied to Battery Research: Hype or Reality? *Chem. Rev.* **2022**, *122* (12), 10899–10969. https://doi.org/10.1021/acs.chemrev.1c00108.
(48) Frazier, P. I. A Tutorial on Bayesian Optimization. arXiv July 8, 2018. https://doi.org/10.48550/arXiv.1807.02811.
(49) Tran, K.; Ulissi, Z. W. Active Learning across Intermetallics to Guide Discovery of Electrocatalysts for CO2 Reduction and H2 Evolution. *Nat. Catal.* **2018**, *1* (9), 696–703. https://doi.org/10.1038/s41929-018-0142-1.
(50) Xu, S.; Li, J.; Cai, P.; Liu, X.; Liu, B.; Wang, X. Self-Improving Photosensitizer Discovery System via Bayesian Search with First-Principle Simulations. *J. Am. Chem. Soc.* **2021**, *143* (47), 19769–19777. https://doi.org/10.1021/jacs.1c08211.
(51) Agarwal, G.; Doan, H. A.; Robertson, L. A.; Zhang, L.; Assary, R. S. Discovery of Energy Storage Molecular Materials Using Quantum Chemistry-Guided Multiobjective Bayesian Optimization. *Chem. Mater.* **2021**, *33* (20), 8133–8144. https://doi.org/10.1021/acs.chemmater.1c02040.
(52) Kim, C.; Chandrasekaran, A.; Jha, A.; Ramprasad, R. Active-Learning and Materials Design: The Example of High Glass Transition Temperature Polymers. *MRS Commun.* **2019**, *9* (3), 860–866. https://doi.org/10.1557/mrc.2019.78.

(53) Nakata, M.; Shimazaki, T. PubChemQC Project: A Large-Scale First-Principles Electronic Structure Database for Data-Driven Chemistry. *J. Chem. Inf. Model.* **2017**, *57* (6), 1300–1308. https://doi.org/10.1021/acs.jcim.7b00083.
(54) Bohacek, R. S.; McMartin, C.; Guida, W. C. The Art and Practice of Structure-Based Drug Design: A Molecular Modeling Perspective. *Med. Res. Rev.* **1996**, *16* (1), 3–50. https://doi.org/10.1002/(SICI)1098-1128(199601)16:1<3::AID-MED1>3.0.CO;2-6.
(55) Nakata, M.; Shimazaki, T.; Hashimoto, M.; Maeda, T. PubChemQC PM6: Data Sets of 221 Million Molecules with Optimized Molecular Geometries and Electronic Properties. *J. Chem. Inf. Model.* **2020**, *60* (12), 5891–5899. https://doi.org/10.1021/acs.jcim.0c00740.
(56) Chen, C.; Ong, S. P. A Universal Graph Deep Learning Interatomic Potential for the Periodic Table. *Nat. Comput. Sci.* **2022**, *2* (11), 718–728. https://doi.org/10.1038/s43588-022-00349-3.
(57) Chen, C.; Ye, W.; Zuo, Y.; Zheng, C.; Ong, S. P. Graph Networks as a Universal Machine Learning Framework for Molecules and Crystals. *Chem. Mater.* **2019**, *31* (9), 3564–3572. https://doi.org/10.1021/acs.chemmater.9b01294.
(58) Gilmer, J.; Schoenholz, S. S.; Riley, P. F.; Vinyals, O.; Dahl, G. E. Neural Message Passing for Quantum Chemistry. In *Proceedings of the 34th International Conference on Machine Learning*; PMLR, 2017; pp 1263–1272.
(59) Duvenaud, D.; Maclaurin, D.; Aguilera-Iparraguirre, J.; Gómez-Bombarelli, R.; Hirzel, T.; Aspuru-Guzik, A.; Adams, R. P. Convolutional Networks on Graphs for Learning Molecular Fingerprints. arXiv November 3, 2015. https://doi.org/10.48550/arXiv.1509.09292.
(60) Deb, K. *Multi-Objective Optimization Using Evolutionary Algorithms*; Wiley, 2001.
(61) Gunantara, N. A Review of Multi-Objective Optimization: Methods and Its Applications. *Cogent Eng.* **2018**, *5* (1), 1502242. https://doi.org/10.1080/23311916.2018.1502242.
(62) Murata, T.; Ishibuchi, H.; Tanaka, H. Multi-Objective Genetic Algorithm and Its Applications to Flowshop Scheduling. *Comput. Ind. Eng.* **1996**, *30* (4), 957–968. https://doi.org/10.1016/0360-8352(96)00045-9.
(63) Maaten, L. van der; Hinton, G. Visualizing Data Using T-SNE. *J. Mach. Learn. Res.* **2008**, *9* (86), 2579–2605.
(64) Pedregosa, F.; Varoquaux, G.; Gramfort, A.; Michel, V.; Thirion, B.; Grisel, O.; Blondel, M.; Prettenhofer, P.; Weiss, R.; Dubourg, V.; Vanderplas, J.; Passos, A.; Cournapeau, D.; Brucher, M.; Perrot, M.; Duchesnay, É. Scikit-Learn: Machine Learning in Python. *J. Mach. Learn. Res.* **2011**, *12* (85), 2825–2830.
(65) Vega, L.; Ruvireta, J.; Viñes, F.; Illas, F. Jacob's Ladder as Sketched by Escher: Assessing the Performance of Broadly Used Density Functionals on Transition Metal Surface Properties. *J. Chem. Theory Comput.* **2018**, *14* (1), 395–403. https://doi.org/10.1021/acs.jctc.7b01047.
(66) Mallikarjun Sharada, S.; Karlsson, R. K. B.; Maimaiti, Y.; Voss, J.; Bligaard, T. Adsorption on Transition Metal Surfaces: Transferability and Accuracy of DFT Using the ADS41 Dataset. *Phys. Rev. B* **2019**, *100* (3), 035439. https://doi.org/10.1103/PhysRevB.100.035439.
(67) Lookman, T.; Balachandran, P. V.; Xue, D.; Yuan, R. Active Learning in Materials Science with Emphasis on Adaptive Sampling Using Uncertainties for Targeted Design. *Npj Comput. Mater.* **2019**, *5* (1), 1–17. https://doi.org/10.1038/s41524-019-0153-8.
(68) Tan, J.; Matz, J.; Dong, P.; Shen, J.; Ye, M. A Growing Appreciation for the Role of LiF in the Solid Electrolyte Interphase. *Adv. Energy Mater.* **2021**, *11* (16), 2100046. https://doi.org/10.1002/aenm.202100046.

(69) von Aspern, N.; Röschenthaler, G.-V.; Winter, M.; Cekic-Laskovic, I. Fluorine and Lithium: Ideal Partners for High-Performance Rechargeable Battery Electrolytes. *Angew. Chem. Int. Ed.* **2019**, *58* (45), 15978–16000. https://doi.org/10.1002/anie.201901381.
(70) Jia, W.; Fan, C.; Wang, L.; Wang, Q.; Zhao, M.; Zhou, A.; Li, J. Extremely Accessible Potassium Nitrate (KNO3) as the Highly Efficient Electrolyte Additive in Lithium Battery. *ACS Appl. Mater. Interfaces* **2016**, *8* (24), 15399–15405. https://doi.org/10.1021/acsami.6b03897.
(71) Wu, F.; Qian, J.; Chen, R.; Lu, J.; Li, L.; Wu, H.; Chen, J.; Zhao, T.; Ye, Y.; Amine, K. An Effective Approach To Protect Lithium Anode and Improve Cycle Performance for Li–S Batteries. *ACS Appl. Mater. Interfaces* **2014**, *6* (17), 15542–15549. https://doi.org/10.1021/am504345s.
(72) Grimme, S.; Antony, J.; Ehrlich, S.; Krieg, H. A Consistent and Accurate Ab Initio Parametrization of Density Functional Dispersion Correction (DFT-D) for the 94 Elements H-Pu. *J. Chem. Phys.* **2010**, *132* (15), 154104. https://doi.org/10.1063/1.3382344.
(73) Ong, S. P.; Richards, W. D.; Jain, A.; Hautier, G.; Kocher, M.; Cholia, S.; Gunter, D.; Chevrier, V. L.; Persson, K. A.; Ceder, G. Python Materials Genomics (Pymatgen): A Robust, Open-Source Python Library for Materials Analysis. *Comput. Mater. Sci.* **2013**, *68*, 314–319. https://doi.org/10.1016/j.commatsci.2012.10.028.
(74) Ramsundar, B.; Eastman, P.; Walters, P.; Pande, V. *Deep Learning for the Life Sciences: Applying Deep Learning to Genomics, Microscopy, Drug Discovery, and More*, 1st edition.; O'Reilly Media: Sebastopol, CA, 2019.
(75) Kendall, A.; Gal, Y. What Uncertainties Do We Need in Bayesian Deep Learning for Computer Vision? arXiv October 5, 2017. https://doi.org/10.48550/arXiv.1703.04977.
(76) Kresse, G.; Furthmüller, J. Efficient Iterative Schemes for Ab Initio Total-Energy Calculations Using a Plane-Wave Basis Set. *Phys. Rev. B* **1996**, *54* (16), 11169–11186. https://doi.org/10.1103/PhysRevB.54.11169.
(77) Kresse, G.; Furthmüller, J. Efficiency of Ab-Initio Total Energy Calculations for Metals and Semiconductors Using a Plane-Wave Basis Set. *Comput. Mater. Sci.* **1996**, *6* (1), 15–50. https://doi.org/10.1016/0927-0256(96)00008-0.
(78) Perdew, J. P.; Burke, K.; Ernzerhof, M. Generalized Gradient Approximation Made Simple. *Phys. Rev. Lett.* **1996**, *77* (18), 3865–3868. https://doi.org/10.1103/PhysRevLett.77.3865.
(79) Kresse, G.; Joubert, D. From Ultrasoft Pseudopotentials to the Projector Augmented-Wave Method. *Phys. Rev. B* **1999**, *59* (3), 1758–1775. https://doi.org/10.1103/PhysRevB.59.1758.
(80) Monkhorst, H. J.; Pack, J. D. Special Points for Brillouin-Zone Integrations. *Phys. Rev. B* **1976**, *13* (12), 5188–5192. https://doi.org/10.1103/PhysRevB.13.5188.

TOC graphic

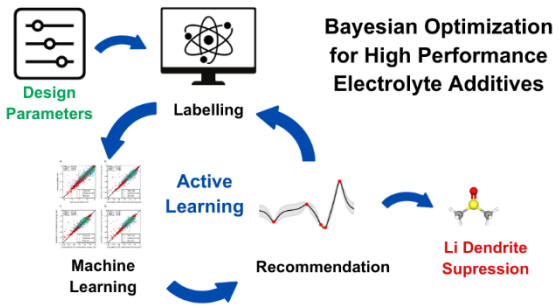
Bayesian Optimization
for High Performance
Electrolyte Additives
Design
Parameters
Labelling
Active
Learning
Machine
Learning
Recommendation
Li Dendrite
Supression